https://doi.org/10.1016/j.marpolbul.2018.12.030

Calcium carbonate unit realignment under acidification: A potential compensatory mechanism in an edible estuarine oyster

Yuan Meng[a], Zhenbin Guo[b], Haimin Yao[b], Kelvin W. K. Yeung[c] and Thiyagarajan V[a,d,*]

[a]The Swire Institute of Marine Sciences and School of Biological Sciences, The University of Hong Kong, Hong Kong SA R, China.

[b]Department of Mechanical Engineering, The Hong Kong Polytechnic University, Hong Kong SAR, China

[c]Department of Orthopaedics and Traumatology, Queen Mary Hospital, The University of Hong Kong, Hong Kong SAR, China.

[d]State Key Laboratory for Marine Pollution, Hong Kong SAR, China

[*]**Corresponding author:**
E-mail address: rajan@hku.hk (Thiyagarajan V.)

Abstract

Ocean acidification (OA) is well-known for impairing marine calcification; however, the end response of several essential species to this perturbation remains unknown. Decreased pH and saturation levels (Ω) of minerals under OA is projected to alter shell crystallography and thus to reduce shell mechanical properties. This study examined this hypothesis using a commercially important estuarine oyster *Magallana hongkongensis*. Although shell damage occurred on the outmost prismatic layer and the undying myostracum at decreased pH 7.6 and 7.3, the major foliated layer was relatively unharmed. Oysters maintained their shell hardness and stiffness through altered crystal unit orientation under pH 7.6 conditions. However, under the undersaturated conditions (Ω_{Cal} ~ 0.8) at pH 7.3, the realigned crystal units in foliated layer ultimately resulted in less stiff shells which indicated although estuarine oysters are mechanically resistant to unfavorable calcification conditions, extremely low pH condition is still a threat to this essential species.

Keywords: ocean acidification, oyster shells, crystallography, mechanical property, calcification, compensatory mechanism.

1 Introduction

Edible oyster species in Chinese coastal areas are belonging to the family *Magallana*, previously *Crassostrea*, and are well known for their ecosystem services such as calcareous reef formation on coastal habitats and for seafood production through aquaculture (Lenihan and Peterson, 1998; Wang et al., 2008; Wang et al., 2010; Zhang et al., 2012). The calcareous shells they produce not only protect their soft tissues but also provide hard substratum for many benthic species. Furthermore, the biologically controlled biomineralization process to produce oyster shells has inspired dentists, material scientists and orthopedics (Fujita et al., 1990; Lee et al., 2008a; Shen et al., 2014). Oyster shells are composites of highly oriented crystal units (>95%) and organic matrix proteins (<5%) (Lee et al., 2008c). Importantly, the assemblage of these two components within a shell is species-specific (Lee et al., 2008b; Lombardi et al., 2013). Depending on the environment and genotype, species assemble crystal units within organic matrix proteins in different ways to maximize mechanical properties with minimal energy expenditure and weight gain (Menig et al., 2000, 2001; Lin et al., 2006). Oysters have a complex life cycle in which the planktotrophic veliger larvae develop for about 2 weeks before becoming pediveliger larvae and metamorphosing into benthic juveniles. The newly attached juveniles form hard and stiff calcareous shells for protection via an energetically expensive and sophisticated biomineralization process, however due to the fragility of these early shells the juvenile oysters remain highly susceptible to predation (Newell et al., 2007). The juvenile oyster's shell is mainly composed of calcite, a less soluble form of calcium carbonate ($CaCO_3$), and a small amount of aragonite, a more soluble form of $CaCO_3$ (Weiner and Addadi, 1997). The complex features and diversity of shell crystal assemblages are a rich source of information for the development of new biomaterials. Nevertheless, the focus of this study is on the environmental implications of shell assemblages.

Like many marine calcifying organisms, oysters depend on their environment for biomineralization, and in current and near-future coastal oceans this can prove challenging. One important component of their environment is the seawater carbonate chemistry, and decreasing pH and carbonate ions due to elevated anthropogenic carbon-dioxide is of greatest concern (Caldeira and Wickett, 2003). Understanding the influence of this change on the end-products of the biomineralization (i.e. shells structure and mechanics) is an important scientific knowledge gap. The elevation of CO_2 in coastal waters triggers a series of chemical

changes through the processes of ocean acidification (OA), which not only depletes resources (i.e. carbonate ion concentration) needed for shell formation but also facilitates the dissolution of formed shells as saturation levels of $CaCO_3$ minerals in the environment decrease (Bednarsek et al., 2012). Consequently, the shell formation processes of several marine calcifying marine organisms, including oysters, is known to be impeded and impaired by OA (Ries, 2011). According to a recent report, exposure of the Pacific oyster, *Magallana gigas* (previously *Crassostrea gigas*) to decreased-pH condition (pH 7.6) altered their energy allocation strategy, shell structural integrity, and finally, reduced shell hardness (Timmins-Schiffman et al., 2014). However, a similar decreased-pH level did not affect shell hardness in juveniles of the estuarine Eastern oyster species, *Crassostrea virginica* (Dickinson et al., 2012; Ivanina et al., 2013). Despite the economic importance of these oysters and the expected threat to the formation of their shells, researchers are only just beginning to understand the effects of OA on oyster shell structure and mechanics.

An oyster shell comprises four mineralized layers: prismatic, foliated, chalky and myostracum (MacDonald et al., 2010). Within the "prominent" foliated layer which is consist of calcite crystal units in elongated foliated laths, the crystal unit's size, shape, and orientation each play an important role in determining the shell's mechanical strength, and thus, the survival of oyster (Lee et al., 2008b; Lee et al., 2008c; Meng et al., 2018). For example, shells with a microstructure that is formed by interlocking and complex crystal units are much stronger than shells of similar size that are formed with straight crystal units. The strong correlation between crystal unit morphology (and orientation) and mechanical strength is expected because resistance to fracture generation increases with decreasing crystal unit size and orientation complexity, as less external force is required for a crack to propagate through larger crystal units. Therefore, it is important to determine the influence of OA on crystal unit morphology, size and orientation and the resulting mechanical properties.

To cope with decreased environmental pH and carbonate ion concentration or saturation state under OA, oysters might allocate more energy toward maintaining the appropriate pH level at the calcification site and to pumping in adequate carbonate ions, against an increasingly unfavorable concentration gradient (Kurihara, 2008; Hofmann and Todgham, 2010). This shift in energy allocation to counter the physiological imbalance at the calcification site may reduce energy available for production of proper biomineralization tools for the assemblage of crystal units in the shell, which could severely affect the

mechanical properties of the shell. For instance, oysters growing in a decreased pH environment may not capable of assembling the mineralized foliated layer properly, which could ultimately reduce the shell hardness and stiffness. However, oysters that inhabit estuarine habitats have higher tolerance ranges in regard to a variety of environmental variables, including pH. Estuarine oysters may, therefore, have physiological or biomineral plasticity allowing them to tolerate decreases in pH, effectively preparing them for the projected environmental change due to OA. In order to explore the tolerance of an estuarine oyster to the CO_2-driven seawater acidification from a biomineralization perspective, we have investigated the effect of OA by using three environmentally and climatically relevant levels of decreased pH as proxy on the structural features of juvenile oyster shells including the microstructure and crystallography, and the mechanical properties of the commercially important oyster, *M. hongkongensis*.

2 Material and Methods

2.1 Experimental animal and design

During the peak reproductive season (June 2016) mature adult oysters (*Magallana hongkongensis*) were collected from an oyster hatchery at the Zhanjiang Research Station (21°20'N, 110°40'E), South China Sea Institute, Chinese Academy of Sciences, China. The brood stock was acclimatized in the laboratory under ambient water conditions (15% salinity, 27°C and $pH_{(NBS)}$ 8.1) for 3 to 4 weeks in large flow-through tanks. Gonads from more than 10 males and females were obtained by "strip spawning" (Dineshram et al., 2013). Fertilization and embryonic development occurred in ambient conditions. At 2 weeks post-fertilization, pediveliger larvae were collected and used in the following pH perturbation experiment.

Three environmentally and climatically representative pH levels (pH 8.1, 7.6 and 7.3) were used to determine the effect of decreased pH or high-CO_2 induced ocean acidification (OA) on the microstructure, crystallography and mechanical properties of juvenile shells. Each of the three pH treatments had three replicate cultures. According to IPCC projections, the average pH in coastal areas may drop to pH 7.9 and 7.6 by the years 2100 and 2300, respectively (IPCC, 2014). The selected decreased pH levels are already ecologically relevant, because the pH of the estuarine habitat where *M. hongkongensis* live naturally fluctuates by as much as 0.5 pH units from the ambient level due to river run off and algal

128 respiration (Dineshram et al., 2013; Duarte et al., 2013; Environmental Protection
129 Department, 2016). The pH perturbation procedure and larval culture techniques have been
130 previously described (Dineshram et al., 2013). Briefly, decreased pH conditions were
131 obtained through bubbling CO_2-enriched air with the appropriate CO_2 concentration. The
132 CO_2 concentration in the bubbled air was adjusted using a dual variable area flow controller
133 (Cole-Parmer Inc.). The pediveliger larvae were randomly distributed among the 12 treatment
134 5L culture tanks (control and 3 treatment pH levels × 3 replicates each, 2~3 larvae ml^{-1} in 5 L
135 buckets, 1 µm filtered seawater, 15 psu salinity, at 27 °C). The tanks were provided with a
136 plastic substrate coated with 7-day-old natural biofilm for attachment and metamorphosis of
137 the pediveliger larvae. The metamorphosed juveniles were transferred 48h-post-settlement
138 and reared under the same pH level for 12 weeks after metamorphosis. Pediveliger larvae and
139 juveniles were fed *ad libitum* with mixed algal cultures (5-10×10^6 cells ml^{-1}) of *Isochrysis*
140 *galbana* and *Chaetoceros gracilis*.

141 Seawater pH (NBS scale) and the temperature were monitored using a Metter-Toledo
142 (SG2) probe and salinity with a refractometer (ATAGO, S/Mill0E; Japan). The probe
143 calibration used NIST buffers (pH =4.01, 7.00, and 9.21; Mettler Toledo, Gmbh Analytical
144 CH8603 Schwerzenbach, Switzerland). In each replicate tank, pH, temperature and salinity
145 were measured daily and averaged within and among days. Afterward, by averaging the
146 replicate culture tanks for each treatment (n = 3), the treatment level (Mean ± SD; Table S1)
147 was calculated. Samples of seawater (50 ml) from each culture tank were collected every two
148 weeks and treated with 10 µl of 250 mM mercuric chloride for total alkalinity (TA) analysis
149 using the Alkalinity Titrator (AC-A2, Apollo SciTech's Inc., U.S.). The TA measurement was
150 standardized with a seawater reference material (Batch 106, A.G. Dickson, Scripps Institution
151 of Oceanography, U.S.). The carbonate system parameters, i.e. carbon dioxide partial
152 pressure (pCO_2; µatm), carbonate ion concentration (CO_3^{2-}; µmol kg^{-1}), calcite and aragonite
153 saturation states (Ω_{Ca}, Ω_{Ar}), were computed using the CO2SYS software program (Pierrot et
154 al., 2006) with equilibrium constants K_1, K_2 and KSO_4 (Mehrbach et al., 1973; Dickson and
155 Millero, 1987) (Table S1). At the end of the experimental period, the juveniles were
156 preserved in 75% ethanol for shell analysis.

157 ***2.2 Shell preparation***

158 Between the two shell valves of the juvenile oyster, the right (or top) valve is responsible
159 for the protection of the soft body from predators and the environmental. Therefore, the top

valve was used in this study to exam the microstructure, crystallography and mechanical properties of the oyster shell using Scanning Electron Microscope imaging (SEM), Electron Back Scatter Diffraction (EBSD) and nanoindentation, respectively. Oyster shells were obtained by carefully removing the soft tissues without damaging the internal surface and airdried before embedding by epoxy resin (EpoxyCure, Buehler). The oyster shell is composed of four layers: prismatic, folia, chalky and myostracum. Among these layers, the foliated layer is a major bulk portion of the shell (Lee et al., 2008b). Therefore, we targeted the foliated layer in examining the effect of decreased pH. The shell was embedded in resin blocks which were then sectioned longitudinally and polished with grit papers (P320, P800, P1200, P2500 and P4000). Further polishing was conducted for 4 minutes on cloths with 1µ and 0.3µ Alpha alumina and 2 minutes with 0.02µ colloidal silica.

2.3 Shell microstructure

The polished smooth surface was etched for 5 minutes using 5 mM ethylenediaminetetraacetic acid (EDTA) for SEM examination (Chan et al., 2012; Fitzer et al., 2014b). After etching, the blocks were mounted and coated with the revealed smooth surfaces mounted upwards on aluminum stubs using carbon tape and painted with silver gel to enhance the conductivity, and then sputter coated with carbon (~50 nm). The microstructures of the oyster shells were observed using on the LEO-1530 Field Emission Gun-Scanning Electron Microscope (FEG-SEM) with a beam voltage of 20 kV (Zeiss, Germany) under an accelerating voltage of 20 kV. The cross-sectional porosity of the foliated layers was calculated using ImageJ software by standardizing and converting an SEM image using thresholding (Hartig, 2013). The pore area was then calculated by using the ImageJ "Analyse Particles" feature due to the divergence in the size of pores. The pore area was measured with a confidence area of > 0.001µm^2. The porosity thresholding was calculated using the non-diffracted regions of images produced by backscattered electrons. Three randomly selected specimens were examined per treatment (one individual per replicate). Kruskal-Wallis tests were used to determine the effect of pH on porosity.

2.4 Crystallographic orientation

Resin blocks without etching were mounted and coated followed the same methodology as described in the previous SEM section. The EBSD measurements were carried out on the LEO-1530 Field Emission Gun-Scanning Electron Microscope (FEG-SEM) with a beam

voltage of 20 kV (Zeiss, Germany) with the stage tilted to 70°. For the EBSD measurement, a step size of 0.5 µm was used. The EBSD data were post-processed using the HKL-Channel 5™ software package and visualized by plotting the crystallographic orientation maps and pole figures that showed the extension of crystallographic orientation. Each color in the maps represents a corresponding crystallographic orientation according to the color key. Three randomly selected specimens were examined per treatment (one individual per replicate).

2.5 Computation of calculated stiffness

The calculated average stiffness of polyphase aggregates of calcitic crystal units in foliated layers with the direction perpendicular to the sectioned surface was computed for each specimen (n = 3) by MTEX, a freely available Matlab© toolbox for quantitative texture analysis (Mainprice et al., 2011) with the anisotropic elastic tensor of single-crystal calcite (Chen et al., 2001) and the crystallographic texture of calcite determined by EBSD based on the same coordinate system.

2.6 Shell mechanical properties

After obtaining a smooth surface from the specimens, load and displacement nanoindentation tests were conducted to determine the mechanical properties of the shell, i.e. hardness and the stiffness (elasticity) (Perez-Huerta et al., 2007). Briefly, nanoindentation tests were carried out using the Hysitron TriboIndenter TI 900 (TI 900, Hysitron, MN, USA) equipped with a Berkovich indenter (a half-angle of 63. 5°). Hardness and stiffness values were calculated based on the loading-unloading curve of each indentation using the Oliver-Pharr model (Doerner and Nix, 1986; Oliver and Pharr, 1992) (Figure S1). The foliated layer in the middle region of the shell was selected as the region of interest to correspond the SEM and EBSD analysis. About 6-10 indents following a matrix-pattern were conducted with a loading of 9000 µN for each. Six specimens of each treatment were randomly selected for nanoindentation tests (two individuals per replicate). Measurements were firstly averaged within each specimen and then by replicate tank. Finally, three values per treatment were obtained (n = 3). All data were tested for normality of residuals, normality, and homogeneity of variance before analyzing by ANOVA. Student-Newman-Keuls test was used to compare the means following one-way ANOVA (Chan et al., 2012).

2.7 Shell mineral density and 3D surface density distribution

The surface topography and the mineral density according to three-dimensional (3D) digital information of the whole oyster juvenile shells were acquired using a high-resolution micro-CT scanning system (SkyScan 1076, Skyscan, Belgium) with a spatial resolution of 9 μm. Each individual air-dried oyster shell was placed on a plastic substrate and put in the chamber of micro-CT scanner. Around 300 two-dimensional (2D) layers were generated from each sample and used to examine the shell density and the volume ratio of partial density after standardization by the phantoms, which is used for bone density calculation, using the analytical software CT-Analyser v 1.14.4.1 (SkyScan, Kontich, Belgium) (Celenk and Celenk, 2012). Reconstruction software CT-Volume v 2.2.1.0 (SkyScan, Kontich, Belgium) was used to convert the 2D layers into a 3D reconstructed model. Three density ranges (0 to 1 g/cm^3, 1 to 2 g/cm^3 and higher than 2 g/cm^3) were selected to represent the high, medium and low density ranges. The volume ratio of the three density ranges were calculated as Volume ratio = Volume of certain density range/Whole shell volume, to investigate the effect of the decreased pH on the shell construction with different density. Three randomly selected specimens (one individual per replicate) were used per treatment (n = 3). All data were tested for normality of residuals, normality, and homogeneity of variance before analyzing by ANOVA. Student-Newman-Keuls test was used to compare the means following one-way ANOVA.

3 Results

3.1 Shell microstructural damage in varying degrees under decreased pH

Irrespective of treatment level, decreased pH resulted in easily observable damage on the outer-most calcitic prismatic layer and the underlying aragonitic myostracum but had a less obvious impact on the “prominent” calcitic foliated layer (Figure 1). The mineral erosion or dissolution was conspicuous on the outer prismatic layer on both the older hinge region and the younger middle region at pH 7.6 and pH 7.3 (Figures 1A-F). Indeed, at the lowest pH, pH 7.3, the prismatic layer was absent from the older hinge and younger middle regions (Figures 1C and F). Similarly, the impact of decreased pH on the myostracum layer which consisted of needle-like aragonitic prims was also prominent (Figures 1G-I). The myostracum prism was shorter and smaller in shape and appeared to be corroded with rounded edges in the treated juvenile shells at pH 7.6 and 7.3 compared with the intact needle-like prims in the control

(Figures 1G-I). However, the impact of decreased pH on the foliated layer, the dominant structure occupied the majority of oyster shell and consisted of calcitic laths, was not clear (Figures 1J-L). The foliated laths were well formed in thickness of approximately 200 nm with a laminated architecture in both decreased pH treatments and control individuals (Figure 1J-L). At the lowest pH 7.3, sporadic gaps were observed between the foliated laths, while those of the shells under the control and the pH 7.6 were packed tightly. In fact, the area porosity of the foliated layer was not affected by the sporadic gaps ($\chi^2_{(2)} = 0.801$, p = 0.073) (Figure 1M). Meanwhile, the chalky layer was not observable in the longitudinal section-surfaces of the juvenile oyster shells from both the control and the decreased pH treatments.

3.2 Less aligned calcite crystal units in foliated layers under decreased pH

The impact of the decreased pH on the crystallographic orientation of the foliated layer is represented by the color change in EBSD crystallographic orientation map (Figures 2i and D). The spread of the data points in the pole figures indicate variation of the *c*-axis of the calcite crystal units (Figures 2ii). In general, the crystallographic *c*-axis across the foliated structure is slightly tilted in the growth direction (elongation of the foliated lath) in both decreased pH treated and control juvenile shells. However, compared with the data points that aggregated with identical orientation from the control shells, there is clearly less constraint on the crystallographic *c*-axis of the calcite units in the juvenile shells grown under both deceased pH treatments (Figures 2ii).

3.3 Decreased pH reduced mechanical properties

Two mechanical properties of shells, hardness and stiffness, were quantitatively measured on the foliated layer using nanoindentation, hereafter as “experimental” hardness and stiffness in Figure 3. Notably, decreased pH treatment levels used in this study did not affect hardness, when compared to control ($F_{(2,6)} = 3.931$, $p = 0.081$) (Figure 3A). Although decreased pH 7.3 significantly reduced the shell stiffness when compared to control shells, the shell stiffness under pH 7.6 was unchanged ($F_{(2,6)} = 6.903$, $p = 0.028$) (Figure 3B). Importantly, the effective stiffness calculated based on the crystallography obtained by EBSD, hereafter as “calculated” stiffness in Figure 3, showed a significant decrease of value at pH 7.3 compared with that at the control pH ($F_{(2,6)} = 5.945$, $p = 0.038$), which agreed with that of the experimental stiffness (Figure 3B).

3.4 Mineral density distribution under the decreased pH

Unlike previous measurements which focus on specific points or regions, the whole shell was assessed for the impact of decreased pH on hard structural features using micro-computed tomography (Micro CT) (Figure 4). The 3D reconstructed model showed that the newly formed edge region and the surface were loaded with low-density materials as represented in red (Figures 4i). Notably, the interior surfaces of shells formed at pH 7.3 and pH 7.6 were loaded with medium- and low-density materials as shown in pink and red colors (Figures 4ii).

The shells fell into three density categories, i.e. < 1g/cm^3, 1-2 g/cm^3 and > 2 g/cm^3. The volume ratio of density less than 1 g/cm^3 in the two decreased pH treatments (pH 7.6 and pH 7.3) was significantly increased compared when compared to control ($F_{(2,6)} = 7.120$, $p = 0.026$) (Figure 4D). There was no significant difference in the volume proportions of the middle (1-2 g/cm^3) and high (> 2 g/cm^3) shell mineral density categories as well as the shell mineral density among pH treatments (Figures 4D and E).

4 Discussion

This study clearly demonstrated the modulating effect of environmental pH and carbonate chemistry associated with OA on structural integrity, crystal unit orientation and mechanical characteristics of an oyster shell. Even a moderate decrease in pH caused structural impairment on the protective outer and inner shell layers, i.e., prismatic and myostracum layers, respectively. In contrast, the inner foliated layer, which makes up the bulk of the shell, was microstructurally intact with “irregularly” aligned calcite crystal units at pH 7.6 and 7.3. The altered crystallography ultimately leads a decrease in stiffness relative to the control, but only in the undersaturated treatment (pH 7.3, $\Omega_{Cal} \sim 0.78$), which coincided with the results of experimental stiffness obtained by nanoindentation. These results provide insight into the biomineralization adaptations of estuarine oysters to tolerate unfavorable calcification conditions, which will be discussed below by revealing the possible linkages between the observed microstructural and mechanical features and also comparing the results with other related studies.

4.1 Structural impairment of oyster shells under decreased pH stress

Except for the invisible chalky layer in the juvenile oyster shells, the other three shell layers, the prismatic, foliated and myostracum exhibited impairment of shell microstructures to varying degrees under decreased pH conditions. Firstly, as expected, the prismatic layer started to dissolve at pH 7.6 and it was completely absent at pH 7.3 (Figures 1A-F). Similar impacts of decreased pH on the prismatic layer were reported for the juvenile scallop, *Argopecten irradians* (Talmage and Gobler, 2010), juvenile hard-shell clams, *Mercenaria mercenaria* (Dickinson et al., 2013) and the rock oyster, *Saccostrea glomerata* (Watson et al., 2009). For outermost mineralized layer, the prismatic layer, dissolution occurred at pH 7.6 with a supersaturated state of calcite (Ω_{Cal}~1.6). Similarly, the dissolution of the prismatic layer in a pteropod shell not only occurred first but also in similarly supersaturated environments (Ω_{Ar}~1.65) (Bednaršek et al., 2012). Therefore, the dissolution of the prismatic layer in this study may be regarded as an initial observable bioindicator of oysters experiencing decreased pH environments.

Secondly, in the myostracum layer the aragonite prisms which are the building blocks were significantly stunted at pH 7.6 (Ω_{Ar}~0.96) and pH 7.3 (Ω_{Ar}~0.47) with an undersaturated state of aragonite. Although the foliated layers were formed with normal microstructures, sporadic gaps between the lath were observed in the calcite undersaturated treatment (pH 7.3, Ω_{Cal}~0.78). According to the molluscan shell calcification process, the mineralization process occurs in compartments with supersaturated conditions at the shell edge (Mount et al., 2004). This means that the newly formed myostracum (or foliated layer), located in the innermost shell surface, is directly exposed to the environment, which may be corrosive and undersaturated (Mount et al., 2004; Toyofuku et al., 2017). The exposed aragonite prisms (or calcite foliated lath) may have been subjected to partial dissolution of the formed crystal units. Similar results were also reported and characterized for the pteropod shell (Bednaršek et al., 2012), mussels (Hahn et al., 2012; Fitzer et al., 2014a) and tubeworms (Li et al., 2014). Therefore, the underlying biomineralized structures with partly eroded building blocks can be regarded as another bioindicator for oysters, representing a more severely deteriorated state caused under OA scenarios.

In addition, these two indicators were verified at a scale that encompassed the entire shell by micro-CT scanning. The overall shell density was not affected, which corroborates the unchanged area porosity of the well-formed foliated layer. However, the increased low-

density volume under decreased pH indicates that shell dissolution may happen for the entire shell, especially for the inner surface that had a density less than 1g/cm^3 in pH 7.3, while it was mostly greater than 2g/cm^3 in the control (Figure 4). During the mineral formation process, marine invertebrates are capable in actively increasing the site of calcification by pumping proton out of the calcification site, thereby enabling calcium carbonate precipitation (Toyofuku et al., 2017). Supersaturated calcite conditions in oyster were found in the restricted compartment around the shell edge including the outer mantle and the first intracellular nucleation site (Mount et al., 2004). Undersaturated calcite conditions may be maintained elsewhere in contact with the inner shell surface (Addadi et al., 2006; Thomsen et al., 2010). This process was recently confirmed in foraminifera, where a dramatic decrease of pH appeared near the nucleation site (Toyofuku et al., 2017).

Therefore, in low pH conditions due to OA, these inner areas of newly formed minerals, which are precipitated as structural building blocks for the prismatic and foliated layers, may still be prone to dissolution. When the shell dissolution rate is faster than the mineralization rate, organisms tend to produce thinner and lighter (less dense) shells resulting in impaired shell microstructure. This may explain the multiple negative effects of reduced pH in our results, including porous and less dense foliated layers

In this way, the inner surface of the oyster shell may be more prone to dissolution because of the decreased pH environment in the calcification compartment or mantle fluid underneath those layers (Melzner et al., 2011). Similar to this study, the serpulid tubeworm, *Hydroides elegans*, showed impaired tube structure with significantly lower density minerals when exposed to decreased pH 7.8 (Li et al., 2014; Li et al., 2016).

4.2 The shell stiffness is highly related to the crystallography under decreased pH

Although there were relatively dramatic damages in the prismatic and myostracum layers under OA scenarios, the foliated layer was formed with well-maintained laminated architecture and complete foliated lath irrespective of treatment levels. However, the calcite crystal units were significantly less aligned in the foliated layer at pH 7.6 and pH 7.3. Marine organisms build their skeletons and shells through aligning crystal units into well-evolved architectures, and the microstructure, organization and orientation of these crystal units determine the ultimate mechanical properties, i.e. stiffness of shells (Rodriguez-Navarro et al., 2002; Agbaje et al., 2017). The foliated layer is the dominant structure that takes up the

majority of this estuarine oysters shell, it consist of calcite crystal units in elongated lath which are separated by small amounts of organic membrane, which is critical for mechanical support and protection (Lee et al., 2011). In order to test if the sporadic gaps affected the entire structure under decreased pH conditions, we quantified the area porosity of the foliated layers. It was showed the area porosity was not affected at low pH, indicating the defects (gaps) of the foliated layer were insufficient to alter the compactness (Figure 1M) of the microstructure and thus the corresponding effectiveness of microstructure on mechanical properties. It may be due to the calcite-based components and their interior position which made the foliated layers less susceptible to the decreased pH conditions, separated from contact with the seawater by the protective prismatic layer. However, the well-formed architecture in the foliated layer is marred by less constrained calcite crystal units, in terms of their crystallographic orientation, at pH 7.6 and 7.3 (Figure 2). Although the impact of OA on crystallography is not well studied, these results are consistent with those of the study in which the blue mussel, *Mytilus edulis* grown under pH 7.5 (750 µatm) and pH 7.3 (1000 µatm) showed less constrained crystallographic orientation compared to those grown in ambient, pH 7.7 (380 µatm), conditions (Fitzer et al., 2014b). Given the high anisotropic stiffness (elastic modulus) of an individual calcite crystal (Chen et al., 2001) and the determining role of crystallography on mechanical properties, the impact of the observed decrease in alignment on shell stiffness was revealed based on the altered crystallography observed in this study. In the same direction perpendicular to the sectioned surface, the changes in the calculated stiffness coincided with the experimental stiffness measured by nanoindentation (Figure 3B), indicating that shell stiffness depends on the aggregation of underlying crystal units. Therefore, based on the above analyses, the impact of decreased environmental pH on the stiffness of foliated layer can be explained by the retained area porosity and the stiffness calculated using crystallography data.

The organic matrix is also a key factor, in addition to microstructure and crystallography, in determining the mechanical properties of the shell (Marin and Luquet, 2004). The involvement of organic constituents in low proportions (0.01 to 5 wt- %) increased the shell fracture toughness of the conch, *Strombus gigas*, by 2 to 3 orders of magnitudes (Kamat et al., 2000). However, the contribution of the organic matrix to the stiffness of the foliated layer in oysters is limited at the micro-meter (nanoindentation) scale and even less than its contribution to hardness. After removing all the organic matrix from the foliated layer of Pacific oyster, *Magallana gigas* (previously *Crassostrea gigas*), the hardness decreased by

405 approximately 27% and the stiffness (elastic modulus) decreased only by 20% (Lee et al.,
406 2008c). Moreover, the density of organic matrix is highly varied across the different shell
407 components within the oyster shell (Dauphin et al., 2013). It is necessary to separate the
408 different shell components to evaluate the contribution of organic matrix to the corresponding
409 mechanical properties of the shell. However, because of the irregular arrangement of the
410 calcitic shells of *Magallana* and the small size of the juvenile shells used in this study, it is
411 not possible to separate the different layers to quantify their mechanical properties and
412 organic components. A future longer-term experiment is needed to harvest shells large
413 enough to investigate the specific matrix proteins packing in each shell structure at the micro
414 or nano-spatial scale, and to illustrate the relationship between shell proteins and the
415 mechanical properties under OA.

416 ### *4.3 A possible compensatory mechanism of M. hongkongensis and the ecological*
417 ### *implications*

418 The result present here showed the shell is damaged to varying degrees on the different
419 structural components of oyster shells, some as sensitive bioindicators showing exposure
420 decreased pH conditions and indicating the inevitable deterioration under OA scenarios.
421 However, the microstructure of the major shell component, the foliated layer, was well-
422 maintained in terms of the fundamental laminated architecture and the integrity of the
423 individual foliated laths used as building blocks. Interestingly, the formation of normal
424 foliated structures was accompanied by a decrease of biological crystallographic control. In
425 foliated layer formation, a well-defined foliated lath is formed by unoriented nanocrystals
426 that contain granulocytic haemocytes (Mount et al., 2004; Johnstone et al., 2015), this is an
427 energy demanding process. With lowered metabolic rates caused by the decreased pH
428 conditions (Dupont and Portner, 2013), energy shortages may occur in oysters, which may
429 limit their control of precipitation, and as we showed, result in the less aligned and controlled
430 calcite crystal units in the foliated layers, which was also apparent in the blue mussel (Fitzer
431 et al., 2014a). Meanwhile, although the altered crystallography ultimately lead to a decrease
432 of stiffness under the most acidified environment at pH 7.3 (Ω_{Cal}~ 0.78), the hardness and
433 stiffness were both retained at pH 7.6 even though the calcite crystal units were also
434 relatively less aligned. Therefore, these less aligned or controlled crystal units may be a
435 compensatory mechanism of *M. hongkongensis*, an estuarine oyster species, to maintain the
436 fundamental microstructure and mechanical properties of the folia layer while at the same

time conserving energy under OA scenarios. This compensatory mechanism may be an adaptation of coastal organisms that experience high fluctuation in coastal and estuarine environments. Similarly, the larvae of the rock oyster, *S. glomerata*, from adults exposed to increasing pCO_2 associated with OA can withstand larger changes than the larvae of wild adults (Parker et al., 2011). Similarly, the results from several other recent studies suggest that organisms living within upwelling environments, such as coastal and estuarine environments, show a degree of adaptation to OA (Wright et al., 2014; Lardies et al., 2017). Consequently, with such adaptations to compensate for fluctuating environments, *M. hongkongensis* in its current state may be sustainable as the dominant species along the southern coast of China.

Nevertheless, given the continuing seawater acidification scenarios and the high fluctuation of seawater chemistry in estuaries (including pH), the survival of *M. hongkongensis* is uncertain in future coastal oceans as the extreme decrease of pH continues. At the lowest pH of 7.3, the less aligned calcite crystals ultimately induced a significant decrease of stiffness, which indicated that the effectiveness of the compensatory mechanism of *M. hongkongensis* can be diminished in more-acidic seawater resulting from continuing OA scenarios. A calcite-based shell is brittle in nature, like egg shells or ceramics, therefore their resistance to deformation (or breaking force) largely depends on its stiffness parameter. The less stiff foliated layer at pH 7.3 may imply an increased susceptibility of these oysters to predators under OA scenarios (Sanford et al., 2014). The initiation of resistance to predation occurs at the post-settlement larval stages and their defences are vital to the oyster population (Newell et al., 2007). The juvenile Olympia oyster, *Ostrea lurida* formed a weaker shells under pH 7.8 and were more prone to being crushed by their predator (Sanford et al., 2014). Consequently, under a predictable long-term scenario, OA may pose a non-negligible threat to the sustainability of the coastal oyster industry and the health of the oyster reef structure.

5 Conflict of Interest

The authors declare no competing or financial interest.

6 Author Contributions

YM and VT conceived and designed the study. ZG and HY performed the nanoindentation test and contributed with materials and analysis equipment. YM performed the CO_2 propagation experiment, SEM and EBSD analyses and contributed to the analysis

equipment. KY contributed with materials and analysis equipment for Micro-CT scanning. YM analyzed the data. YM and VT drafted the manuscript.

7 Funding

This work was supported by a grant from the HKSAR-RGC (No. 17304914 and 17303517).

8 Acknowledgments

The authors would like to thank Shu Xiao and Yu Ziniu of South China Sea Institute of Oceanology, Chinese Academy of Sciences (Guangzhou, China) for providing brood stocks for this work and for their assistance with the oyster culture. We also would like to thank Maggie Cusack, Susan Fitzer and Vera BS Chan for their comments on the data analysis and interpretation of EBSD data. We acknowledge the University of Hong Kong-EMU facility for help with the SEM and EBSD analysis. Thanks to Y.Y. Chui (University of Hong Kong, HKU) for sectioning and Tony Liu on micro-CT work.

481 **References**

482 Addadi, L., Joester, D., Nudelman, F., Weiner, S., 2006. Mollusk shell formation: a source of
483 new concepts for understanding biomineralization processes. Chem. Eur. J. 12, 980-987.
484 http://dx.doi.org/10.1002/chem.200500980.

485 Agbaje, O.B.A., Wirth, R., Morales, L.F.G., Shirai, K., Kosnik, M., Watanabe, T., Jacob,
486 D.E., 2017. Architecture of crossed-lamellar bivalve shells: the southern giant clam
487 (*Tridacna derasa*, Röding, 1798). R. Soc. Open Sci. 4.
488 http://dx.doi.org/10.1098/rsos.170622.

489 Bednaršek, N., Tarling, G.A., Bakker, D.C.E., Fielding, S., Cohen, A., Kuzirian, A.,
490 McCorkle, D., Lézé, B., Montagna, R., 2012. Description and quantification of pteropod
491 shell dissolution: a sensitive bioindicator of ocean acidification. Glob. Chang. Biol. 18,
492 2378-2388. http://dx.doi.org/10.1111/j.1365-2486.2012.02668.x.

493 Bednarsek, N., Tarling, G.A., Bakker, D.C.E., Fielding, S., Jones, E.M., Venables, H.J.,
494 Ward, P., Kuzirian, A., Leze, B., Feely, R.A., et al., 2012. Extensive dissolution of live
495 pteropods in the Southern Ocean. Nat. Geosci. 5, 881-885.
496 http://dx.doi.org/10.1038/ngeo1635.

497 Caldeira, K., Wickett, M.E., 2003. Anthropogenic carbon and ocean pH. Nature 425, 365.
498 http://dx.doi.org/10.1038/425365a.

499 Celenk, C., Celenk, P., 2012. Bone density measurement using computed tomography, in:
500 Saba, L. (Ed.), Computed Tomography - Clinical Applications. InTech, Rijeka, Croatia,
501 pp. 123-136.

502 Chan, V.B., Li, C., Lane, A.C., Wang, Y., Lu, X., Shih, K., Zhang, T., Thiyagarajan, V.,
503 2012. CO_2-driven ocean acidification alters and weakens integrity of the calcareous tubes
504 produced by the serpulid tubeworm, *Hydroides elegans*. PloS ONE 7, e42718.
505 http://dx.doi.org/10.1371/journal.pone.0042718.

506 Chen, C.C., Lin, C.C., Liu, L.G., Sinogeikin, S.V., Bass, J.D., 2001. Elasticity of single-
507 crystal calcite and rhodochrosite by Brillouin spectroscopy. Am. Mineral. 86, 1525-1529.
508 http://dx.doi.org/10.2138/am-2001-11-1222.

509 Dauphin, Y., Ball, A.D., Castillo-Michel, H., Chevallard, C., Cuif, J.-P., Farre, B., Pouvreau,
510 S., Salomé, M., 2013. *In situ* distribution and characterization of the organic content of
511 the oyster shell *Crassostrea gigas* (Mollusca, Bivalvia). Micron 44, 373-383.
512 http://dx.doi.org/10.1016/j.micron.2012.09.002.

513 Dickinson, G.H., Ivanina, A.V., Matoo, O.B., Portner, H.O., Lannig, G., Bock, C., Beniash,
514 E., Sokolova, I.M., 2012. Interactive effects of salinity and elevated CO_2 levels on
515 juvenile eastern oysters, *Crassostrea virginica*. J. Exp. Biol. 215, 29-43.
516 http://dx.doi.org/10.1242/jeb.061481.
517 Dickinson, G.H., Matoo, O.B., Tourek, R.T., Sokolova, I.M., Beniash, E., 2013.
518 Environmental salinity modulates the effects of elevated CO_2 levels on juvenile hard-
519 shell clams, *Mercenaria mercenaria*. J. Exp. Biol. 216, 2607-2618.
520 http://dx.doi.org/10.1242/jeb.082909.
521 Dickson, A.G., Millero, F.J., 1987. A comparison of the equilibrium constants for the
522 dissociation of carbonic acid in seawater media. Deep Sea Res. (I Oceanogr. Res. Pap.)
523 34, 1733-1743. http://dx.doi.org/10.1016/0198-0149(87)90021-5.
524 Dineshram, R., Thiyagarajan, V., Lane, A., Yu, Z., Xiao, S., Leung, P.T.Y., 2013. Elevated
525 CO_2 alters larval proteome and its phosphorylation status in the commercial oyster,
526 *Crassostrea hongkongensis*. Mar. Biol. 160 2189-2205 http://dx.doi.org/10.1007/s00227-
527 013-2176-x.
528 Doerner, M.F., Nix, W.D., 1986. A method for interpreting the data from depth-sensing
529 indentation instruments. J. Mater. Res. 1, 601-609.
530 http://dx.doi.org/10.1557/JMR.1986.0601.
531 Duarte, C.M., Hendriks, I.E., Moore, T.S., Olsen, Y.S., Steckbauer, A., Ramajo, L.,
532 Carstensen, J., Trotter, J.A., McCulloch, M., 2013. Is ocean acidification an ppen-ocean
533 syndrome? Understanding anthropogenic impacts on seawater pH. Estuar. Coast. 36,
534 221-236. http://dx.doi.org/10.1007/s12237-013-9594-3.
535 Dupont, S., Portner, H., 2013. Marine science: Get ready for ocean acidification. Nature 498,
536 429-429. http://dx.doi.org/10.1038/498429a.
537 Environmental Protection Department, 2016. Marine Water Quality Data, Hong Kong
538 Special Administrative Region, China.
539 Fine, M., Tchernov, D., 2007. Scleractinian Coral Species Survive and Recover from
540 Decalcification. Science 315, 1811-1811. http://dx.doi.org/10.1126/science.1137094.
541 Fitzer, S.C., Cusack, M., Phoenix, V.R., Kamenos, N.A., 2014a. Ocean acidification reduces
542 the crystallographic control in juvenile mussel shells. J. Struct. Biol. 188, 39-45.
543 http://dx.doi.org/10.1016/j.jsb.2014.08.007.
544 Fitzer, S.C., Phoenix, V.R., Cusack, M., Kamenos, N.A., 2014b. Ocean acidification impacts
545 mussel control on biomineralisation. Sci. Rep. 4, 6218.
546 http://dx.doi.org/10.1038/srep06218.

547 Fujita, T., Fukase, M., Miyamoto, H., Matsumoto, T., Ohue, T., 1990. Increase of bone
548 mineral density by calcium supplement with oyster shell electrolysate. Bone Miner. 11,
549 85-91. http://dx.doi.org/10.1016/0169-6009(90)90017-A.
550 Hahn, S., Rodolfo-Metalpa, R., Griesshaber, E., Schmahl, W.W., Buhl, D., Hall-Spencer,
551 J.M., Baggini, C., Fehr, K.T., Immenhauser, A., 2012. Marine bivalve shell geochemistry
552 and ultrastructure from modern low pH environments: environmental effect versus
553 experimental bias. Biogeosciences 9, 1897-1914. http://dx.doi.org/10.5194/bg-9-1897-
554 2012.
555 Hartig, S.M., 2013. Basic Image Analysis and Manipulation in ImageJ. Curr. Protoc. Mol.
556 Biol. 102, 14.15.11-14.15.12. http://dx.doi.org/doi:10.1002/0471142727.mb1415s102.
557 Hofmann, G.E., Todgham, A.E., 2010. Living in the Now: Physiological Mechanisms to
558 Tolerate a Rapidly Changing Environment. Annu. Rev. Physiol. 72, 127-145.
559 http://dx.doi.org/10.1146/annurev-physiol-021909-135900.
560 IPCC, 2014. Climate Change 2014: Synthesis Report. Contribution of Working Groups I, II
561 and III to the Fifth Assessment Report of the Intergovernmental Panel on Climate
562 Change. , in: Core Writing Team, R.L.P., and L. A. Meyer. (Ed.). IPCC, Geneva,
563 Switzerland., p. 151.
564 Ivanina, A.V., Dickinson, G.H., Matoo, O.B., Bagwe, R., Dickinson, A., Beniash, E.,
565 Sokolova, I.M., 2013. Interactive effects of elevated temperature and CO_2 levels on
566 energy metabolism and biomineralization of marine bivalves *Crassostrea virginica* and
567 *Mercenaria mercenaria*. Comp. Biochem. Physiol. A Mol. Integr. Physiol. 166, 101-111.
568 http://dx.doi.org/10.1016/j.cbpa.2013.05.016.
569 Johnstone, M.B., Gohad, N.V., Falwell, E.P., Hansen, D.C., Hansen, K.M., Mount, A.S.,
570 2015. Cellular orchestrated biomineralization of crystalline composites on implant
571 surfaces by the eastern oyster, *Crassostrea virginica* (Gmelin, 1791). J. Exp. Mar. Bio.
572 Ecol. 463, 8-16. http://dx.doi.org/10.1016/j.jembe.2014.10.014.
573 Kamat, S., Su, X., Ballarini, R., Heuer, A.H., 2000. Structural basis for the fracture toughness
574 of the shell of the conch *Strombus gigas*. Nature 405, 1036-1040.
575 http://dx.doi.org/10.1038/35016535.
576 Kurihara, H., 2008. Effects of CO_2-driven ocean acidification on the early developmental
577 stages of invertebrates. Mar. Ecol. Prog. Ser. 373, 275-284.
578 http://dx.doi.org/10.3354/meps07802.
579 Lardies, M.A., Benitez, S., Osores, S., Vargas, C.A., Duarte, C., Lohrmann, K.B., Lagos,
580 N.A., 2017. Physiological and histopathological impacts of increased carbon dioxide and

581 temperature on the scallops *Argopecten purpuratus* cultured under upwelling influences
582 in northern Chile. Aquaculture 479, 455-466.
583 http://dx.doi.org/10.1016/j.aquaculture.2017.06.008.
584 Lee, C.H., Lee, D.K., Ali, M.A., Kim, P.J., 2008a. Effects of oyster shell on soil chemical
585 and biological properties and cabbage productivity as a liming materials. Waste
586 Management 28, 2702-2708. http://dx.doi.org/10.1016/j.wasman.2007.12.005.
587 Lee, S.W., Jang, Y.N., Ryu, K.W., Chae, S.C., Lee, Y.H., Jeon, C.W., 2011. Mechanical
588 characteristics and morphological effect of complex crossed structure in biomaterials:
589 fracture mechanics and microstructure of chalky layer in oyster shell. Micron 42, 60-70.
590 http://dx.doi.org/10.1016/j.micron.2010.08.001.
591 Lee, S.W., Kim, G.H., Choi, C.S., 2008b. Characteristic crystal orientation of folia in oyster
592 shell, *Crassostrea gigas*. Mater. Sci. Eng. C Biomimetic Supramol. Syst. 28, 258-263.
593 http://dx.doi.org/10.1016/j.msec.2007.01.001.
594 Lee, S.W., Kim, Y.M., Kim, R.H., Choi, C.S., 2008c. Nano-structured biogenic calcite: A
595 thermal and chemical approach to folia in oyster shell. Micron 39, 380-386.
596 http://dx.doi.org/10.1016/j.micron.2007.03.006.
597 Lenihan, H.S., Peterson, C.H., 1998. How habitat degradation through fishery disturbance
598 enchances impacts of hypoxia on oyster reefs. Ecol. Appl. 8, 128-140.
599 http://dx.doi.org/10.1890/1051-0761(1998)008[0128:HHDTFD]2.0.CO;2.
600 Li, C., Chan, V.B.S., He, C., Meng, Y., Yao, H., Shih, K., Thiyagarajan, V., 2014.
601 Weakening mechanisms of the serpulid tube in a high-CO_2 world. Environ. Sci. Technol.
602 48, 14158-14167. http://dx.doi.org/10.1021/es501638h.
603 Li, C., Meng, Y., He, C., Chan, V.B.S., Yao, H., Thiyagarajan, V., 2016. Mechanical
604 robustness of the calcareous tubeworm *Hydroides elegans*: warming mitigates the
605 adverse effects of ocean acidification. Biofouling 32, 191-204.
606 http://dx.doi.org/10.1080/08927014.2015.1129532.
607 Lin, A.Y.M., Meyers, M.A., Vecchio, K.S., 2006. Mechanical properties and structure of
608 *Strombus gigas*, *Tridacna gigas*, and *Haliotis rufescens* sea shells: A comparative study.
609 Materials Science and Engineering: C 26, 1380-1389.
610 http://dx.doi.org/10.1016/j.msec.2005.08.016.
611 Lombardi, S.A., Chon, G.D., Lee, J.J.W., Lane, H.A., Paynter, K.T., 2013. Shell hardness
612 and compressive strength of the eastern oyster, *Crassostrea virginica*, and the asian
613 oyster, *Crassostrea ariakensis*. Biol. Bull. 225, 175-183.
614 http://dx.doi.org/10.1086/BBLv225n3p175.

615 MacDonald, J., Freer, A., Cusack, M., 2010. Alignment of crystallographic *c*-axis throughout
616 the four distinct microstructural layers of the oyster *Crassostrea gigas*. Cryst. Growth
617 Des. 10, 1243-1246. http://dx.doi.org/10.1021/cg901263p.
618 Mainprice, D., Hielscher, R., Schaeben, H., 2011. Calculating anisotropic physical properties
619 from texture data using the MTEX open-source package. Geol. Soc. Lond. Spec. Publ.
620 360, 175-192. http://dx.doi.org/10.1144/SP360.10.
621 Marin, F., Luquet, G., 2004. Molluscan shell proteins. C. R. Palevol 3, 469-492.
622 http://dx.doi.org/10.1016/j.crpv.2004.07.009.
623 Mehrbach, C., Culberson, C.H., Hawley, J.E., Pytkowicx, R.M., 1973. Measurement of the
624 apparent dissociation constants of carbonic acid in seawater at atmospheric pressure.
625 Limnol. Oceanogr. 18, 897-907. http://dx.doi.org/10.4319/lo.1973.18.6.0897.
626 Melzner, F., Stange, P., Trübenbach, K., Thomsen, J., Casties, I., Panknin, U., Gorb, S.N.,
627 Gutowska, M.A., 2011. Food supply and seawater pCO_2 impact calcification and internal
628 shell dissolution in the blue mussel *Mytilus edulis*. PloS ONE 6, e24223.
629 http://dx.doi.org/10.1371/journal.pone.0024223.
630 Meng, Y., Fitzer, S.C., Chung, P., Li, C.Y., Thiyagarajan, V., Cusack, M., 2018.
631 Crystallographic Interdigitation in Oyster Shell Folia Enhances Material Strength. Cryst.
632 Growth Des. 18, 3753-3761. http://dx.doi.org/10.1021/acs.cgd.7b01481.
633 Menig, R., Meyers, M.H., Meyers, M.A., Vecchio, K.S., 2000. Quasi-static and dynamic
634 mechanical response of *Haliotis rufescens* (abalone) shells. Acta Mater. 48, 2383-2398.
635 http://dx.doi.org/10.1016/S1359-6454(99)00443-7.
636 Menig, R., Meyers, M.H., Meyers, M.A., Vecchio, K.S., 2001. Quasi-static and dynamic
637 mechanical response of *Strombus gigas* (conch) shells. Mater. Sci. Eng., A 297, 203-211.
638 http://dx.doi.org/10.1016/S0921-5093(00)01228-4.
639 Mount, A.S., Wheeler, A.P., Paradkar, R.P., Snider, D., 2004. Hemocyte-mediated shell
640 mineralization in the eastern oyster. Science 304, 297-300.
641 http://dx.doi.org/10.1126/science.1090506.
642 Newell, R.I.E., Kennedy, V.S., Shaw, K.S., 2007. Comparative vulnerability to predators, and
643 induced defense responses, of eastern oysters *Crassostrea virginica* and non-native
644 *Crassostrea ariakensis* oysters in Chesapeake Bay. Mar. Biol. 152, 449-460.
645 http://dx.doi.org/10.1007/s00227-007-0706-0.
646 Oliver, W.C., Pharr, G.M., 1992. An improved technique for determining hardness and
647 elastic modulus using load and displacement sensing indentation experiments. J. Mater.
648 Res. 7, 1564-1583. http://dx.doi.org/10.1557/JMR.1992.1564.

649 Parker, L.M., Ross, P.M., O'Connor, W.A., 2011. Populations of the Sydney rock oyster,
650 Saccostrea glomerata, vary in response to ocean acidification. Mar. Biol. 158, 689-697.
651 http://dx.doi.org/10.1007/s00227-010-1592-4.
652 Perez-Huerta, A., Cusack, M., 2009. Optimizing electron backscatter diffraction of carbonate
653 biominerals-resin type and carbon coating. Microsc. Microanal. 15, 197-203.
654 http://dx.doi.org/10.1017/S1431927609090370.
655 Perez-Huerta, A., Cusack, M., Zhu, W., England, J., Hughes, J., 2007. Material properties of
656 brachiopod shell ultrastructure by nanoindentation. J. R. Soc. Lond. Interface 4, 33-39.
657 http://dx.doi.org/10.1098/rsif.2006.0150.
658 Pierrot, D., Lewis, E., Wallace, D., 2006. MS Excel program developed for CO_2 system
659 calculations. ORNL/CDIAC-105a. Carbon Dioxide Information Analysis Center, Oak
660 Ridge National Laboratory, US Department of Energy, Oak Ridge, Tennessee.
661 Ries, J.B., 2011. Skeletal mineralogy in a high-CO_2 world. J. Exp. Mar. Bio. Ecol. 403, 54-
662 64. http://dx.doi.org/10.1016/j.jembe.2011.04.006.
663 Rodriguez-Navarro, A., Kalin, O., Nys, Y., Garcia-Ruiz, J.M., 2002. Influence of the
664 microstructure on the shell strength of eggs laid by hens of different ages. Br. Poult. Sci.
665 43, 395-403. http://dx.doi.org/10.1080/00071660120103675.
666 Sanford, E., Gaylord, B., Hettinger, A., Lenz, E.A., Meyer, K., Hill, T.M., 2014. Ocean
667 acidification increases the vulnerability of native oysters to predation by invasive snails.
668 Proc. R. Soc. London, Ser. B 281, 20132681. http://dx.doi.org/10.1098/rspb.2013.2681.
669 Shen, Y., Yang, S., Liu, J., Xu, H., Shi, Z., Lin, Z., Ying, X., Guo, P., Lin, T., Yan, S., et al.,
670 2014. Engineering Scaffolds Integrated with Calcium Sulfate and Oyster Shell for
671 Enhanced Bone Tissue Regeneration. ACS Appl. Mater. Interfaces 6, 12177-12188.
672 http://dx.doi.org/10.1021/am501448t.
673 Talmage, S.C., Gobler, C.J., 2010. Effects of past, present, and future ocean carbon dioxide
674 concentrations on the growth and survival of larval shellfish. Proc. Natl. Acad. Sci. 107,
675 17246-17251. http://dx.doi.org/10.1073/pnas.0913804107.
676 Thomsen, J., Gutowska, M.A., Saphörster, J., Heinemann, A., Trübenbach, K., Fietzke, J.,
677 Hiebenthal, C., Eisenhauer, A., Körtzinger, A., Wahl, M., et al., 2010. Calcifying
678 invertebrates succeed in a naturally CO_2-rich coastal habitat but are threatened by high
679 levels of future acidification. Biogeosciences 7, 3879-3891. http://dx.doi.org/10.5194/bg-
680 7-3879-2010.
681 Timmins-Schiffman, E., Coffey, W.D., Hua, W., Nunn, B.L., Dickinson, G.H., Roberts, S.B.,
682 2014. Shotgun proteomics reveals physiological response to ocean acidification in

683 *Crassostrea gigas*. BMC Genomics 15, 951. http://dx.doi.org/10.1186/1471-2164-15-
684 951.
685 Toyofuku, T., Matsuo, M.Y., de Nooijer, L.J., Nagai, Y., Kawada, S., Fujita, K., Reichart, G.-
686 J., Nomaki, H., Tsuchiya, M., Sakaguchi, H., et al., 2017. Proton pumping accompanies
687 calcification in foraminifera. Nat. Commun. 8, 14145.
688 http://dx.doi.org/10.1038/ncomms14145.
689 Wang, H., Qian, L., Liu, X., Zhang, G., Guo, X., 2010. Classification of a Common Cupped
690 Oyster from Southern China. J. Shellfish Res. 29, 857-866.
691 http://dx.doi.org/10.2983/035.029.0420.
692 Wang, H., Zhang, G., Liu, X., Guo, X., 2008. Classification of Common Oysters from North
693 China. J. Shellfish Res. 27, 495-503. http://dx.doi.org/10.2983/0730-
694 8000(2008)27[495:COCOFN]2.0.CO;2.
695 Watson, S.-A., Southgate, P.C., Tyler, P.A., Peck, L.S., 2009. Early larval development of the
696 Sydney rock oyster *Saccostrea glomerata* under near-future predictions of CO_2-driven
697 ocean acidification. J. Shellfish Res. 28, 431-437.
698 http://dx.doi.org/10.2983/035.028.0302.
699 Weiner, S., Addadi, L., 1997. Design strategies in mineralized biological materials. J. Mater.
700 Chem. 7, 689-702. http://dx.doi.org/DOI: 10.1039/A604512J.
701 Wright, J.M., Parker, L.M., O'Connor, W.A., Williams, M., Kube, P., Ross, P.M., 2014.
702 Populations of Pacific oysters *Crassostrea gigas* respond variably to elevated CO_2 and
703 predation by *Morula marginalba*. Biol. Bull. 226, 269-281.
704 http://dx.doi.org/10.1086/BBLv226n3p269.
705 Zhang, G., Fang, X., Guo, X., Li, L., Luo, R., Xu, F., Yang, P., Zhang, L., Wang, X., Qi, H.,
706 et al., 2012. The oyster genome reveals stress adaptation and complexity of shell
707 formation. Nature 490, 49. http://dx.doi.org/10.1038/nature11413.

708

709

710 **Figures**

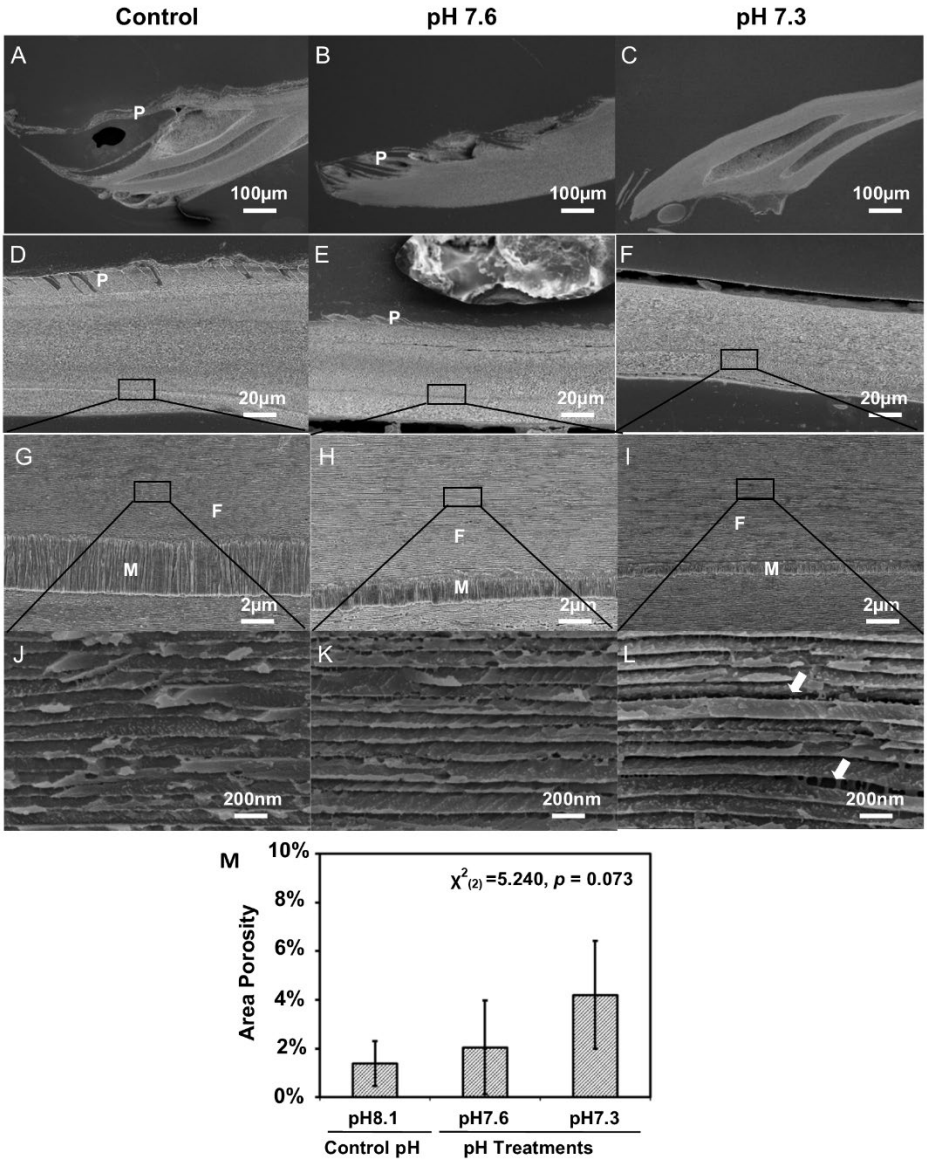

711

712 **Figure 1** Scanning electron micrographs from the cross-sectional surfaces of juvenile
713 *Magallana hongkongensis* shells cultured in the control pH 8.1 (A, D, G and J), treatment pH
714 7.6 (B, E, H and K) and pH 7.3 (C, F, I and L) were compared. First row: scanning electron
715 micrographs taken near the older hinge region (A-C). Second row: scanning electron
716 micrographs taken near the younger middle region (D-F). Compare with the prismatic layer
717 in the control (A and D), the prismatic layers have partially lost at pH 7.6 (B and E) and were
718 not detectable at pH 7.3 (C and F) on both regions. Third row: well-formed myostracum at
719 the control pH of 8.1 (G) and narrower myostracum with stunted aragonite prims at pH 7.6
720 (H) and pH 7.3 (I). Fourth row: enlarged views of the foliated layer at the control (J), pH 7.6
721 (K) and pH 7.3 (L). (M): The area porosity of foliated layers under the control and decreased

pH conditions. The mean values are presented in the bar chart (mean ± SD, n = 3). Annotations: P- prismatic layer; M- myostracum; F- foliated layer. White arrow: irregular gaping of the foliated layer.

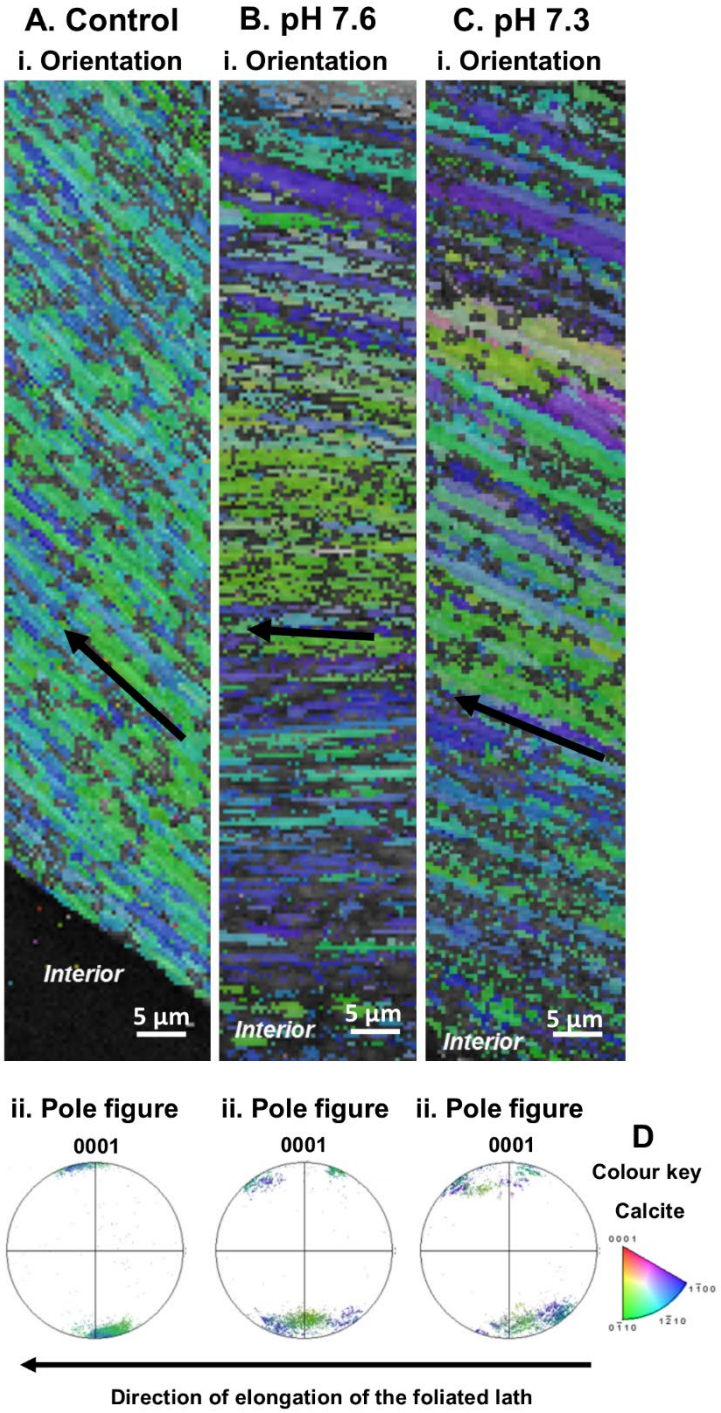

Figure 2 Electron backscatter diffraction analyses of shells grown at ambient or control pH 8.1 (A), treatment pH 7.6 (B) and pH 7.3 (C). Crystallographic orientation map (i) of calcite crystals of shell foliated layer in reference to the {0001} plane. Crystallographic

planes of calcite are color-coded linked to the normal crystallographic direction using the color key (Perez-Huerta and Cusack, 2009Perez-Huerta and Cusack, 2009) (D). Pole figures for calcite (ii) with the direction of elongation of the foliated lath correspond to the crystallographic orientation maps and used the same color key. Black arrow: the direction of elongation of the foliated layer. Scale bar = 5 μm.

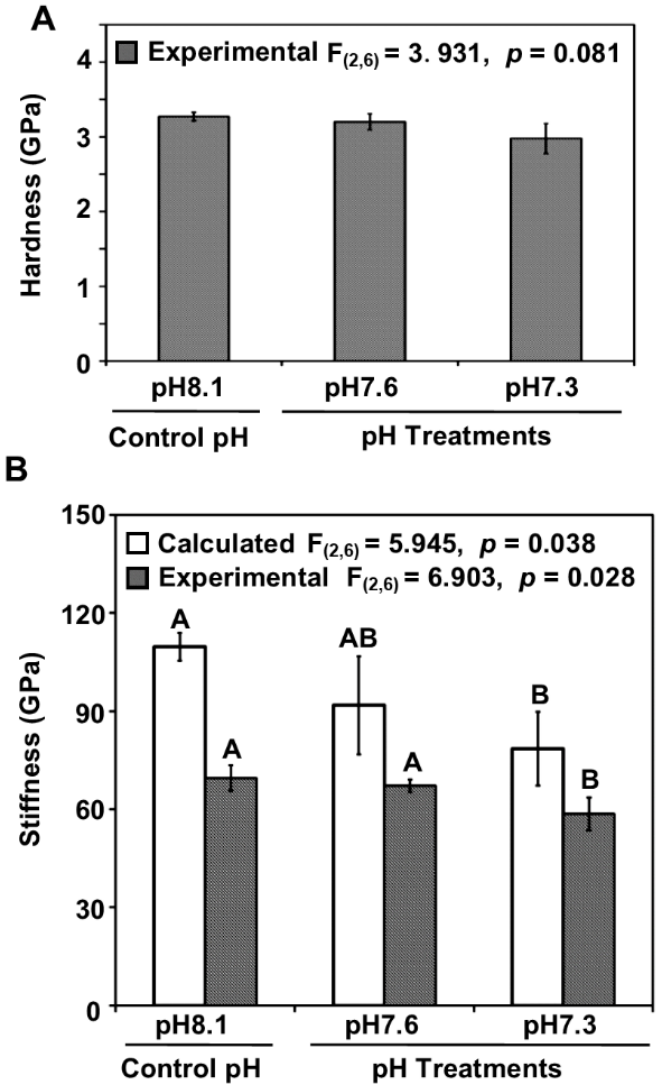

Figure 3 The impact of the decreased pH conditions on the shell mechanical properties in terms of hardness (A) and stiffness (B) of *Magallana hongkongensis* from the cross-sectional surfaces were compared. The experimental hardness and stiffness were measured by nanoindentation in cross-sectional shell surfaces of *Magallana hongkongensis*. The calculated stiffness was computed based on the crystallography in the same direction. Data of mechanical properties are presented as mean ± SD of three replicates (n = 3). Different

741 capital case letters illustrate significant differences ($p < 0.05$) among treatments found
742 through comparisons Student-Newman-Keuls test following a one-way ANOVA.

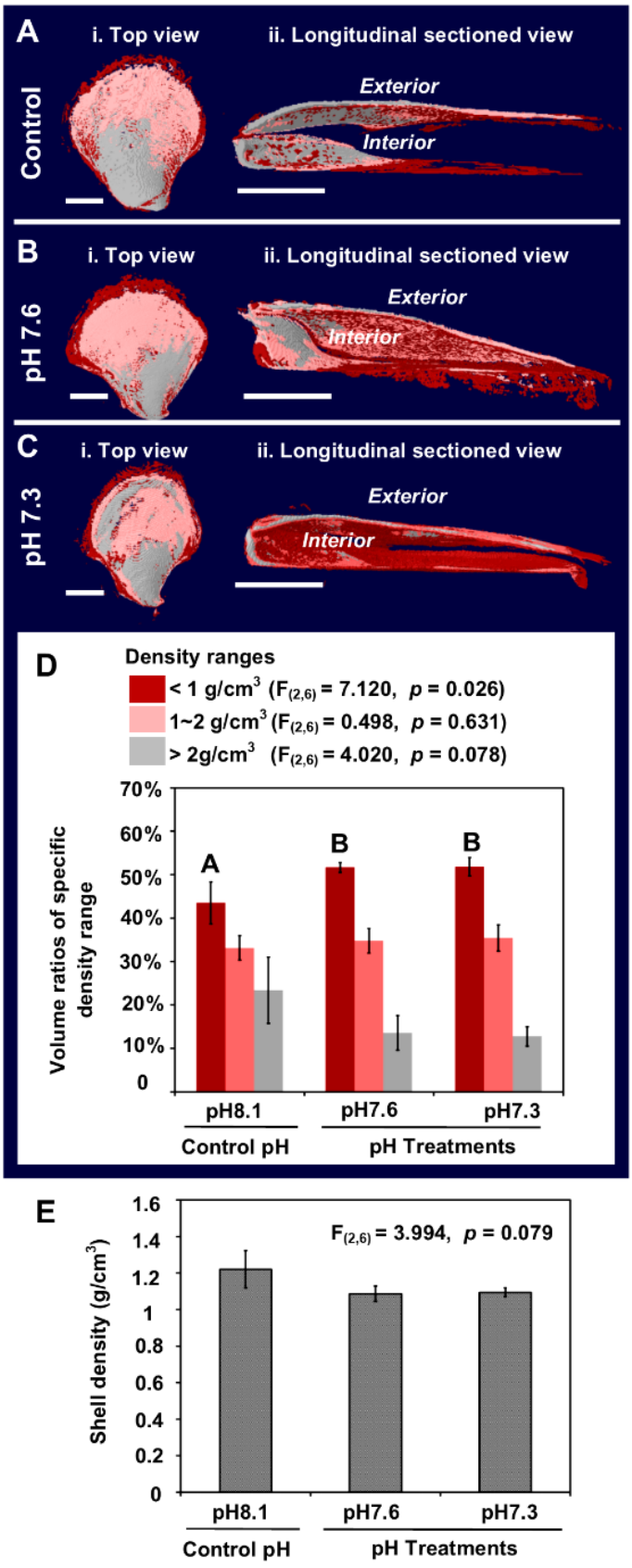

743

744 **Figure 4** The impact of the decreased pH conditions on the shell density of *Magallana*
745 *hongkongensis* cultured under at ambient or control pH 8.1 (A), treatment pH 7.6 (B) and pH
746 7.3 (C) from the top view (i) and the longitudinally sectioned view (ii) are reconstructed and
747 showed representative by the micro-CT scans. The impact of the decreased pH conditions on
748 the shell volume ratio of partial density categories (D), and overall density (E) are examined.
749 The volume ratio of partial density categories was quantified, i.e. <1 g/cm^3, 1-2 g/cm^3 and >
750 2 g/cm^3. The mean values were presented in a bar chart (mean ± SD, n = 3). Scale bar = 3
751 mm